Pergamon

PII: S0301-9322(96)00024-9

Int. J. Multiphase Flow Vol. 22, No. 5, pp. 909–922, 1996

0301-9322/96 $15.00 + 0.00

STUDY OF THE BEHAVIOR OF A BUBBLE ATTACHED TO A WALL IN A UNIFORM ELECTRIC FIELD

H. J. CHO[1], I. S. KANG[1], Y. C. KWEON[2] and M. H. KIM[2]

[1]Department of Chemical Engineering, POSTECH, San 31, Hyojadong, Pohang, 790-784, Korea

[2]Department of Mechanical Engineering, POSTECH, San 31, Hyojadong, Pohang, 790-784, Korea

(Received 13 April 1995; in revised form 19 April 1996)

Abstract—In order to investigate the effects of a uniform electric field on a bubble attached to a wall, numerical analyses and experiments have been carried out. The orthogonal curvilinear coordinate system generated numerically has been employed for the numerical studies based on a finite-difference solution of the governing equations. The steady bubble shape is obtained under the fixed contact radius condition as part of the solution of the free boundary problem. Along with the shape determination, the Laplace equation for electric potential is solved simultaneously. In experimental studies, an air bubble attached to one plate of a parallel-plate electrode system has been visualized under an applied electric field. The numerical and experimental results show generally good agreements. An air bubble on the lower electrode is found to be extended in the direction parallel to the applied electric field. The elongation increases with an increase of the electric field strength. Consequently, the contact angle also increases with an increase of the electric field strength if the contact radius is fixed. On the other hand, if the contact angle is fixed, the contact radius decreases as the electric field strength increases. It has been observed experimentally that the bubble departure volume remains nearly constant under the uniform electric field. This fact suggests that the downward electric force exerted on the bubble surface is nearly the same as the decrease in the surface tension force due to contact radius decrease under the uniform electric field. Copyright © 1996 Elsevier Science Ltd.

Key Words: electrohydrodynamics, bubble, contact angle, aspect ratio, bubble departure volume

1. INTRODUCTION

It has long been established that the basic studies for the effect of an electric field on gas bubbles or liquid drops play an important role for understanding in the areas of heat and mass transfer augmentation. The fundamental researches on the electrohydrodynamic (EHD) enhancement of transport process can be largely classified into two groups: studies on the freely suspended bubbles/drops and studies on the bubbles/drops attached to a wall.

Owing to potential applications to the industrial situation, numerous theoretical and experimental analyses have been conducted in the last few decades to investigate the effects of an electric field on the behavior of a freely suspended bubble/drop in an infinite medium. These works have been well documented in references (Cheng & Chaddock 1984; Chang & Berg 1985; Feng & Beard 1991; Wohlhuter & Basaran 1992; He & Chang 1995).

In order to explain the electrohydrodynamic enhancement of boiling heat transfer from the heating surface, a great deal of experimental studies have been carried out for an attached bubble (Bonjour *et al.* 1962; Markel & Durfee 1965; Lovenguth & Hanesian 1971; Zanin 1987). It has been revealed from the experimental results that the applied electric field affects the basic mechanisms of the nucleate boiling such as bubble formation, growth and departure from the heating surface. Some major effects of an applied electric field include the increase in the number of boiling bubbles, the decrease of the bubble departure volume, and the increase of maximum heat flux (Choi 1962; Jones 1978; Allen *et al.* 1987; Cooper 1990; Ogata & Yabe 1991). Based on these experimental observations, it has been suggested that mutual interaction between a dielectric liquid and an imposing electric field leads to change in the bubble dynamics on the heating surface, which is believed to be one of the main causes of the boiling heat transfer enhancement. However, the

basic mechanisms of heat transfer enhancement by application of an electric field have hardly been clarified yet. The boiling heat transfer problem is a free boundary problem in which the gas–liquid interface shape is unknown *a priori* but must be determined as part of solution of nonlinear equations. Due to the intrinsic difficulty in the problem, only very few theoretical studies have been performed.

Recently, Cheng & Chaddock (1986) have examined the bubble departure size in a uniform electric field. They used the spheroidal approximation of bubble shape and the free energy minimization condition to calculate the equilibrium profile of a bubble. Their results show that the bubble departure size decreases with an increase of the dimensionless electric field strength. In the basic experiment on the behavior of an air bubble in DC electric field, Ogata & Yabe (1993) observed elongation and horizontal motion of a bubble on the plate. They analysed this behavior by considering the electric potential distribution and the electric force around a spheroidally approximated bubble. However, their analyses are not rigorous in the sense that they are based on the spheroidal approximation for a freely suspended bubble in an infinite medium. Since the works of Cheng & Chaddock and Ogata & Yabe, no further attempt to study the behavior of an attached bubble in the presence of an electric field has been reported. Thus, there has been a need for a rigorous study of bubble behavior which is obtained without making approximations on the bubble shape such as the spheroidal approximation.

In the present study, numerical analyses and experiments have been performed to investigate the effects of a uniform electric field on the behavior of a bubble attached to a wall. The bubble shape and electric field are determined simultaneously by solving the governing equations on a numerically generated orthogonal curvilinear coordinate system. In our numerical studies, a bubble with a fixed contact area is considered in order to maintain the consistency with the experimental condition. In experiments, an air bubble attached to the lower flat electrode is visualized under an applied electric field.

2. PROBLEM STATEMENT

In order to study the effects of a DC electric field on a bubble, we consider a gas bubble attached to a wall as shown in figure 1. In the figure, x and σ are the rotational axis and the radial coordinate of the cylindrical coordinate system and $r = (x^2 + \sigma^2)^{1/2}$. The bubble volume is assumed to be $\frac{2}{3}\pi a^3$, where a is the radius of an equivalent hemispherical bubble attached to a wall. The bubble surface is assumed to be characterized by a uniform surface tension γ and the bubble is assumed to sit on the conducting flat wall with contact angle θ_c and contact radius r_c. The electrical conductivity and permittivity of the gas inside the bubble are assumed to be negligible in comparison with those of the surrounding liquid. The surrounding liquid is assumed to be incompressible and it is also

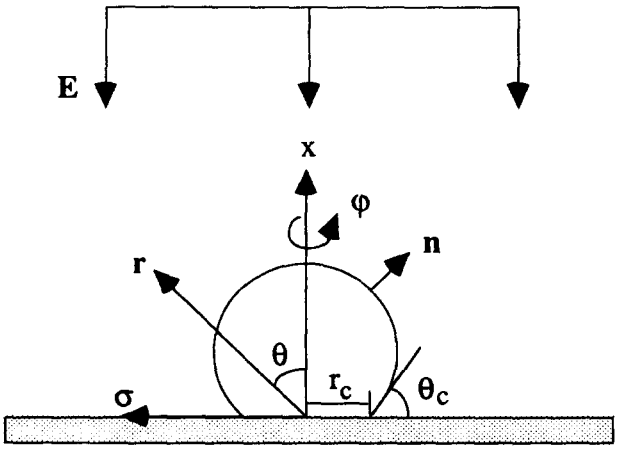

Figure 1. A bubble attached to a wall in a uniform electric field.

assumed that there is no bulk free charge in the surrounding liquid. The applied electric field far from the bubble is uniform in space and constant in time. The far field can be expressed in terms of the electric potential, which is defined by $E_\infty = -\nabla\phi_\infty$, as

$$\phi_\infty = -E_\infty r\cos\theta, \tag{1}$$

where θ is the angle measured from the symmetric axis.

As mentioned above, it is assumed that there is no bulk free charge in the surrounding liquid. Thus, the electric potential around a bubble satisfies the Laplace equation

$$\nabla^2\phi = 0 \tag{2}$$

and the boundary conditions

$$\phi \to -E_\infty r\cos\theta \text{ as } r\to\infty, \tag{3}$$

$$\mathbf{n}\cdot\nabla\phi = 0 \text{ on the bubble surface,} \tag{4}$$

$$\phi = 0 \text{ at } \theta = \frac{\pi}{2}(x=0), \tag{5}$$

where $\mathbf{n}$ is the outgoing unit normal vector from the bubble surface. Equation [4] is the condition that the normal component of the current vector ($\mathbf{J}_f = \sigma_c\mathbf{E}$) vanishes at the insulating interface. Equation [5] is the condition that the surface potential of a conducting electrode must be uniform.

The bubble shape is determined by the normal stress condition

$$p_{in} - p_{out} + \mathbf{n}\cdot(\mathbf{n}\cdot\mathbf{T}^e)_{out} = \gamma(\nabla\cdot\mathbf{n}), \tag{6}$$

where p_{out} is simply redefined by addition of an electrically induced pressure based on the incompressibility assumption for the surrounding liquid. Hence we ignore electrostriction forces as in Melcher & Taylor (1969). The Maxwell stress tensor $\mathbf{T}^e$ is defined by

$$\mathbf{T}^e = \epsilon\mathbf{E}\mathbf{E} - \tfrac{1}{2}\epsilon E^2\mathbf{I}, \tag{7}$$

where ϵ is the permittivity and E is the magnitude of $\mathbf{E}$. Therefore the normal stress condition is given by

$$-\Delta p_0 + \Delta\rho g x - \tfrac{1}{2}\epsilon E_t^2 = \gamma(\nabla\cdot\mathbf{n}), \tag{8}$$

where Δp_0 is the pressure difference at $x=0$, $\Delta\rho$ the density difference, and E_t the tangential component of the electric field.

To non-dimensionalize the governing equations and boundary conditions, we introduce the following characteristic scales

$$l_c = a, \quad \phi_c = E_\infty l_c. \tag{9}$$

Then the dimensionless governing equation and boundary conditions are (we adopt the same notations for the dimensionless variables as dimensional ones if not confused)

$$\nabla^2\phi = 0, \tag{10}$$

with

$$\phi \to -x \text{ as } r\to\infty, \tag{11}$$

$$\mathbf{n}\cdot\nabla\phi = 0 \text{ on the bubble surface,} \tag{12}$$

$$\phi = 0 \text{ at } \theta = \frac{\pi}{2}(x=0). \tag{13}$$

The dimensionless normal stress condition is

$$-N_p + N_g x - \frac{N_e}{2} E_t^2 = (\nabla \cdot \mathbf{n}), \qquad [14]$$

where $N_p = \Delta p_0 a/\gamma$ and $N_g = \Delta \rho g a^2/\gamma$. The constant N_p is determined by the constraint of constant bubble volume $V_0 = 2\pi/3$ based on the incompressibility assumption of gas inside the bubble. The relative importance of gravity and surface tension effects on the bubble shape is represented by N_g, which is called the gravity–capillary number (Crowley 1995). For large bubbles, the gravity effect dominates, while for small bubbles the surface tension effect will play a significant role in determination of static bubble shape. Another dimensionless number of importance in [14] is N_e, which is defined by $N_e = \epsilon E_\infty^2 a/\gamma$ and called the electrical Weber number.

In this work, the free boundary problem defined by [10]–[14] has been solved numerically by using the orthogonal grid generation method. To corroborate the numerical results, experiments have also been performed.

3. NUMERICAL SCHEME

In free boundary problems, the boundary shape is not known *a priori* but must be determined as part of solution. In many cases, the boundary shape is determined iteratively starting from a certain initial shape. This iteration procedure may be incorporated with the grid generation technique with an adjustable function that modifies the boundary shape. In fact, the method of orthogonal grid generation has been successfully applied for various free boundary problems such as deformation of a bubble (Kang & Leal 1987). In this section, the basic idea of grid generation method of Ryskin & Leal (1983) is briefly reviewed. The global solution scheme to obtain the electric potential with determination of bubble shape will also be presented.

3.1. Orthogonal grid generation

The numerical generation of a boundary-fitted orthogonal coordinate system is illustrated in figure 2. Taking advantage of the symmetry in the problem, we consider only half of the problem domain. Since the physical domain (x, σ) outside the bubble is an infinite domain, we consider instead an auxiliary finite domain (x^*, σ^*) that can be obtained by inverse conformal mapping

$$x + i\sigma = \frac{1}{x^* - i\sigma^*}. \qquad [15]$$

The orthogonal mapping between (x^*, σ^*) domain and the computational (ξ, η) domain can be found by solving the covariant Laplace equations

$$\frac{\partial}{\partial \xi}\left(f \frac{\partial x^*}{\partial \xi}\right) + \frac{\partial}{\partial \eta}\left(\frac{1}{f} \frac{\partial x^*}{\partial \eta}\right) = 0, \qquad [16]$$

$$\frac{\partial}{\partial \xi}\left(f \frac{\partial \sigma^*}{\partial \xi}\right) + \frac{\partial}{\partial \eta}\left(\frac{1}{f} \frac{\partial \sigma^*}{\partial \eta}\right) = 0, \qquad [17]$$

with suitable boundary conditions. In the above equations, $f(\xi, \eta)$ is the distortion function defined as the ratio of two scale factors, $f(\xi, \eta) \equiv h_\eta^*/h_\xi^*$. The scale factors are defined by

$$h_\xi^* = \left[\left(\frac{\partial x^*}{\partial \xi}\right)^2 + \left(\frac{\partial \sigma^*}{\partial \xi}\right)^2\right]^{1/2}, \qquad [18]$$

$$h_\eta^* = \left[\left(\frac{\partial x^*}{\partial \eta}\right)^2 + \left(\frac{\partial \sigma^*}{\partial \eta}\right)^2\right]^{1/2}. \qquad [19]$$

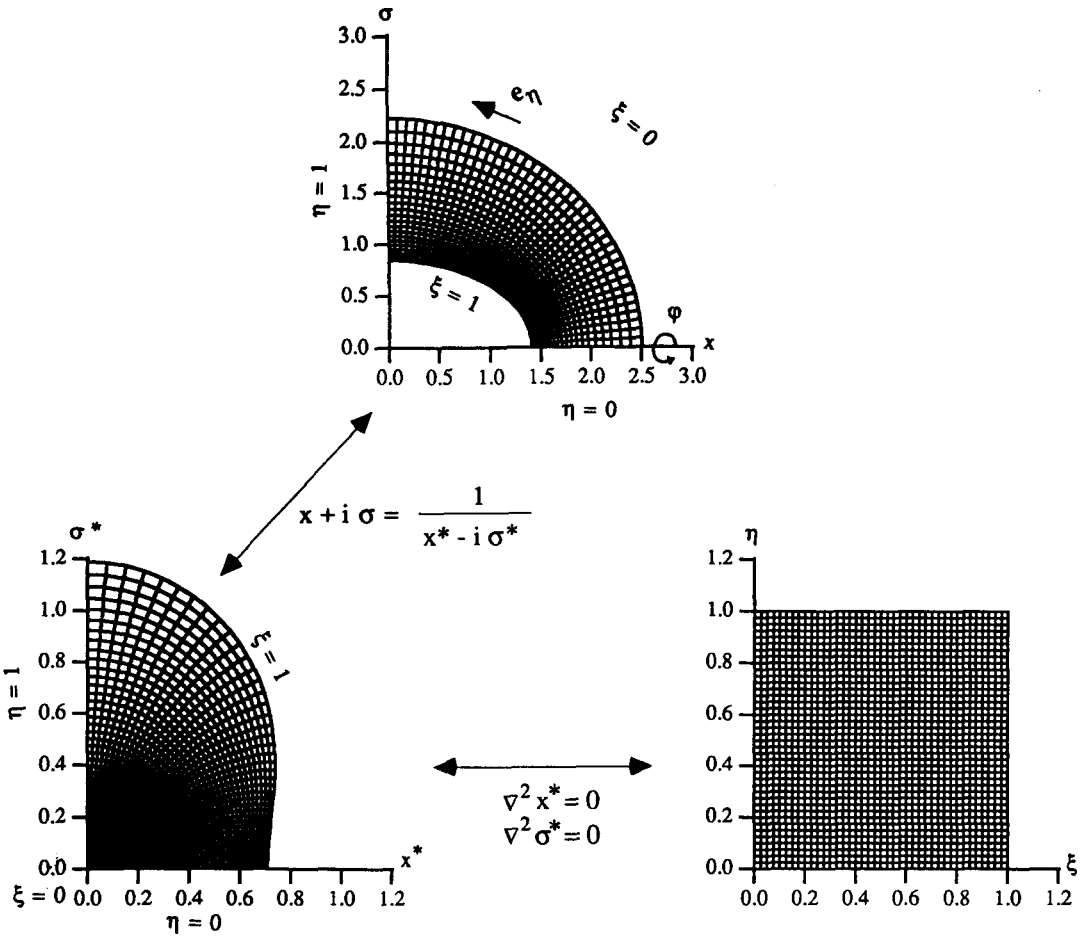

Figure 2. Orthogonal mapping of the (x, σ) domain onto (ξ, η) domain.

In our computation, we have used the specified function $f(\xi, \eta) = \pi\xi/2$ to make [16] and [17] determinate. As we may note from the definition of $h_\xi^*(1, \eta)$, it represents the grid spacing in the normal direction at the boundary. Once $h_\xi^*(1, \eta)$ is specified, the boundary shape is automatically determined in the process of adjustment of grid spacing to satisfy the governing equations and boundary conditions (see Ryskin & Leal 1984). The grid system for an infinite domain outside the bubble can easily be obtained by inverting the (x^*, σ^*) domain conformally.

3.2. *Governing equations and boundary conditions in the orthogonal coordinate system*

In axisymmetric orthogonal coordinates, the Laplace equation for the electric potential around a bubble ϕ is expressed as (Batchelor 1967)

$$\frac{\partial}{\partial\xi}\left(\frac{h_\eta\sigma}{h_\xi}\frac{\partial\phi}{\partial\xi}\right) + \frac{\partial}{\partial\eta}\left(\frac{h_\xi\sigma}{h_\eta}\frac{\partial\phi}{\partial\eta}\right) = 0. \qquad [20]$$

The numerical scheme for solving the Laplace equation [20] (or [10] in vector form) with boundary conditions [11], [12] and [13] is straightforward except that the electric potential becomes unbounded as $r \to \infty$ (i.e. $\phi \to -x$ as $r \to \infty$). In order to avoid the difficulty arising from the singularity at infinity, we define a function ϕ^* as $\phi^* = \phi - \phi_0$, where ϕ_0 is an unbounded function

such that $\phi_0 \to -x$. Therefore we can assume $\phi^* \to 0$ as $r \to \infty$. One of the most convenient choices for ϕ_0 is the solution for the electrostatic field around a spherical bubble

$$\phi_0 = -\left(\frac{1}{2r^2} + r\right)\cos\theta = -x\left(\frac{1}{2r^3} + 1\right). \quad [21]$$

Using the relation $\phi = \phi^* + \phi_0$, we obtain the governing equation for ϕ^* in orthogonal coordinates given by

$$\frac{\partial}{\partial\xi}\left(\frac{h_\eta\sigma}{h_\xi}\frac{\partial\phi^*}{\partial\xi}\right) + \frac{\partial}{\partial\eta}\left(\frac{h_\xi\sigma}{h_\eta}\frac{\partial\phi^*}{\partial\eta}\right) = -\frac{\partial}{\partial\xi}\left(\frac{h_\eta\sigma}{h_\xi}\frac{\partial\phi_0}{\partial\xi}\right) - \frac{\partial}{\partial\eta}\left(\frac{h_\xi\sigma}{h_\eta}\frac{\partial\phi_0}{\partial\eta}\right), \quad [22]$$

with the boundary conditions

$$\phi^* = 0 \text{ at } \xi = 0, \quad [23]$$

$$\frac{\partial\phi^*}{\partial\xi} = -\frac{\partial\phi_0}{\partial\xi} \text{ at } \xi = 1, \quad [24]$$

$$\frac{\partial\phi^*}{\partial\eta} = -\frac{\partial\phi_0}{\partial\eta} \text{ at } \eta = 0, \quad [25]$$

$$\phi^* = 0 \text{ at } \eta = 1. \quad [26]$$

In order to determine the bubble shape in an electric field, we need to consider the normal stress balance at the surface. From [14], the normal stress condition can be applied to the bubble surface in the form

$$-N_p + N_g x - \frac{N_e}{2}E_\eta^2 - (\kappa_{(\eta)} + \kappa_{(\varphi)}) = 0, \quad [27]$$

where

$$E_\eta = \frac{1}{h_\eta}\frac{\partial\phi}{\partial\eta}.$$

In [27], $\kappa_{(\eta)}$ and $\kappa_{(\varphi)}$ denote the curvatures in $\mathbf{e}_{(\eta)}$ and $\mathbf{e}_{(\varphi)}$ directions and for axisymmetric orthogonal coordinate system they are given by

$$\kappa_{(\eta)} = \frac{1}{h_\eta^3}\left(\frac{\partial x}{\partial\eta}\frac{\partial^2\sigma}{\partial\eta^2} - \frac{\partial^2 x}{\partial\eta^2}\frac{\partial\sigma}{\partial\eta}\right), \quad \kappa_{(\varphi)} = -\frac{1}{h_\eta\sigma}\frac{\partial x}{\partial\eta}. \quad [28]$$

In addition to the normal stress condition, we use the constant volume constraint to determine the bubble shape. Since we assume that the bubble volume is fixed, the value of N_p in [27] must be determined in a way to satisfy the following condition at the bubble surface

$$V = \left|\pi\int_0^1\left(\sigma^2\frac{\partial x}{\partial\eta}\right)d\eta\right| = \text{const.} \quad [29]$$

The detailed procedure to determine the bubble shape will be discussed in the following section.

3.3. *Shape determination*

The bubble deformation occurs in a way to satisfy the normal stress balance. Thus, we first calculate the normal stress imbalance along the given bubble surface. Then the bubble surface is

adjusted to minimize the normal stress imbalance. Since $h_\xi^*(1, \eta)$ is the control function for the shape change, we must devise a relationship between $h_\xi^*(1, \eta)$ and the normal stress imbalance along the bubble surface. When the bubble volume is fixed with V_0, the bubble shape is determined during the iteration by adjusting the shape control function as

$$h_\xi^{*(n+1)}(1, \eta) = \left(\frac{V^{(n)}}{V_0}\right)^{1/3} h_\xi^{*(n)}(1, \eta) - \beta r^{*2}(\Pi(\eta) - \bar{\Pi})^{(n)}, \quad [30]$$

where β is a positive relaxation parameter and $\Pi(\eta) - \bar{\Pi}$ is the excess normal stress at $\xi = 1$ calculated by

$$\Pi(\eta) = \frac{N_g}{N_e} x - \frac{1}{2}E_\eta^2 - \frac{1}{N_e}(\kappa_{(\eta)} + \kappa_{(\varphi)}), \quad [31]$$

and

$$\bar{\Pi} = \frac{\int_0^1 \Pi(\eta)\sigma h_\eta \, d\eta}{\int_0^1 \sigma h_\eta \, d\eta}. \quad [32]$$

The bubble shape determination procedure is very similar to that in Ryskin & Leal (1984).

3.4. *The global numerical procedure*

For the free-boundary problem, all equations for x^*, σ^*, ϕ are solved simultaneously with determination of the boundary shape. The procedure is iterated until the fully converged solutions of the electric field and the coordinate system are attained. The flow sheet for the global numerical scheme is shown in figure 3.

4. EXPERIMENTAL APPARATUS AND PROCEDURE

Figure 4 shows a schematic diagram of the experimental system. The apparatus consists of two copper flat electrodes with dimensions 120 mm × 120 mm, DC high voltage power supply, the high voltage probe and the test chamber made with tempered glass to facilitate visual observations. An air bubble is generated through the stainless steel tube with inner diameter 0.1 mm and outer diameter 0.71 mm and is injected to surrounding dielectric fluid, cyclohexane, C_6H_{12}. The physical properties of cyclohexane are listed in table 1. The air filter dryer is used to remove the moisture and the foreign substances within air. Since the conductivity of dried air is less than 10^{-14} S/m (i.e. $\sigma_c < 10^{-14}$ S/m), the ratio of conductivity of air to that of cyclohexane is less than 10^{-3} and it satisfies the assumptions made in the problem statement. The copper plate electrode is first polished with emery paper (no. 1000), then polished with 1 μm Al_2O_3, and finally rinsed with acetone. The experiments are carried out changing the applied voltage from 0 to 30 kV by DC power supply. The high voltage probe is used to measure the high voltage applied on the electrode accurately. The DC high voltage is applied to the upper electrode, while the lower electrode is grounded, so that an electric field between the upper and lower electrodes is built. The electric field between two parallel-plate electrodes is nearly uniform. In order to visualize the bubble shape in an electric field, back and side light methods with an extension lens and reflecting screen are used.

5. RESULTS AND DISCUSSION

In numerical computation, the contact radius r_c is assumed to be fixed to compare the numerical results with the experimental results for an air bubble attached to the lower flat electrode under the electric field. Figure 5 shows the equipotential lines around an insulating bubble attached to

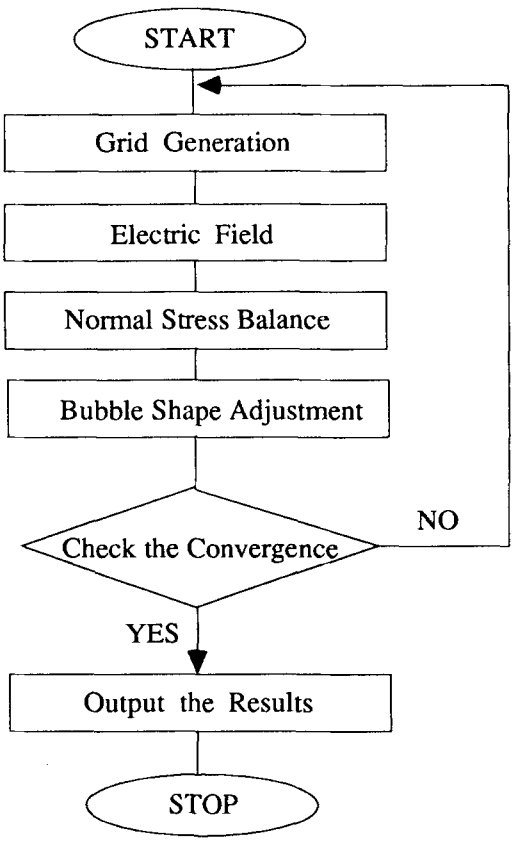

Figure 3. Flow chart of the numerical analysis.

the flat wall when $N_g = 0.0$, $r_c/a = 0.8$, $N_e = 2.0$. As shown in the figure, the equipotential lines become curved near the bubble surface to satisfy the boundary condition $\partial\phi/\partial n = 0$ and the electric field becomes stronger near the bubble than far from the bubble.

In figure 6, the evolution of bubble shape with increasing N_e is shown for the case of fixed contact radius $r_c/a = 0.535$, $N_g = 0.18$ (these values were chosen from the experimental conditions). As in the case of a freely suspended bubble in an infinite medium, a bubble becomes more extended in

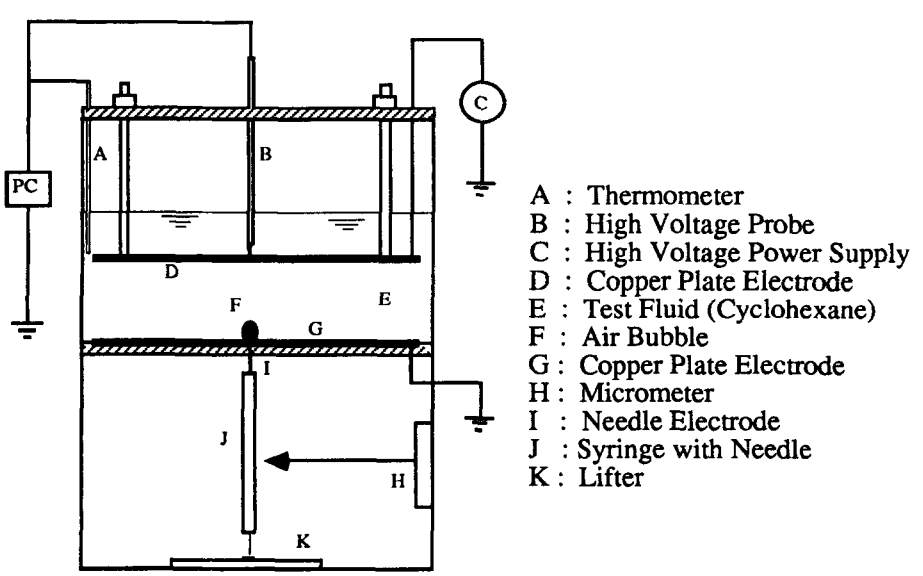

Figure 4. Schematic diagram of the experimental apparatus.

Table 1. Properties of C_6H_{12} at 20°C

ρ (density)	949 kg/m^3
μ (viscosity)	0.92E-3 Ns/m^2
ϵ (permittivity)	1.948E-11 F/m
γ (surface tension)	2.45E-2 N/m
σ_e (conductivity)	2.5E-11 S/m

(Ref. Kagaku Binran, 2nd Ed. Maruzen)

the direction parallel to the imposed electric field as the electric field strength increases. The numerically obtained bubble shapes are very similar to those from the experimental visualization of an air bubble on the lower electrode under a uniform electric field shown in figure 7. From figures 6 and 7, it is shown that a larger deformation of an air bubble is obtained for larger N_e.

When the contact radius is fixed during deformation, the imposed electric field also affects the contact angle θ_c. Figure 8 shows variation of the contact angle with the increase of N_e. From the experimental and numerical results, it is observed that the contact angle increases with an increase of N_e. In figure 9, the variation of the relative aspect ratio $(AR)_e/(AR)_0$ can be seen, where $(AR)_0$ represents the aspect ratio of the undeformed bubble in the absence of an electric field. The relative aspect ratio increases almost linearly with the increase of N_e. From the figure, we can see that the numerical results show a good agreement with the experimental results at least up to $N_e = 2.0$. On the other hand, the prediction from the spheroidal approximation (Cheng & Chaddock 1986) deviates considerably from the experimental results if $N_e \geqslant 1.0$. This fact may explain that the analysis based on the spheroidal approximation has some limitations in the study for deformation of a bubble attached to a wall.

In figure 10, the numerical results for the contact angle as a function of the contact radius for several values of N_e are presented. From the figure, we can see that the contact angle increases with the increase of electric field strength if the contact radius is fixed. On the other hand, the effect of an electric field can be equivalently represented by the change in the contact radius for a fixed contact angle. As we can see in figure 10, the contact radius decreases with the increase of N_e when the contact angle is fixed.

The bubble departure volume is also affected by the electric field. When an electric field is applied, the force balance on a bubble for departure may be represented as

$$F_b = F_s + F_e, \qquad [33]$$

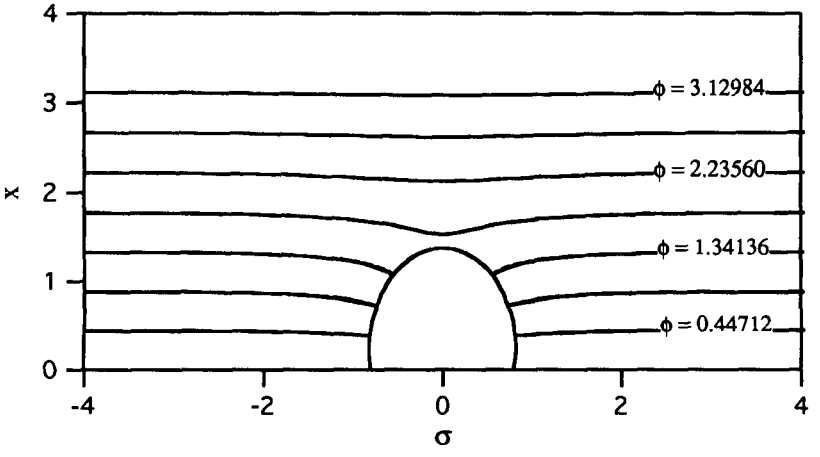

Figure 5. Equipotential lines around a deformed bubble attached to a wall ($r_c/a = 0.8$, $N_g = 0.0$, $N_e = 2.0$).

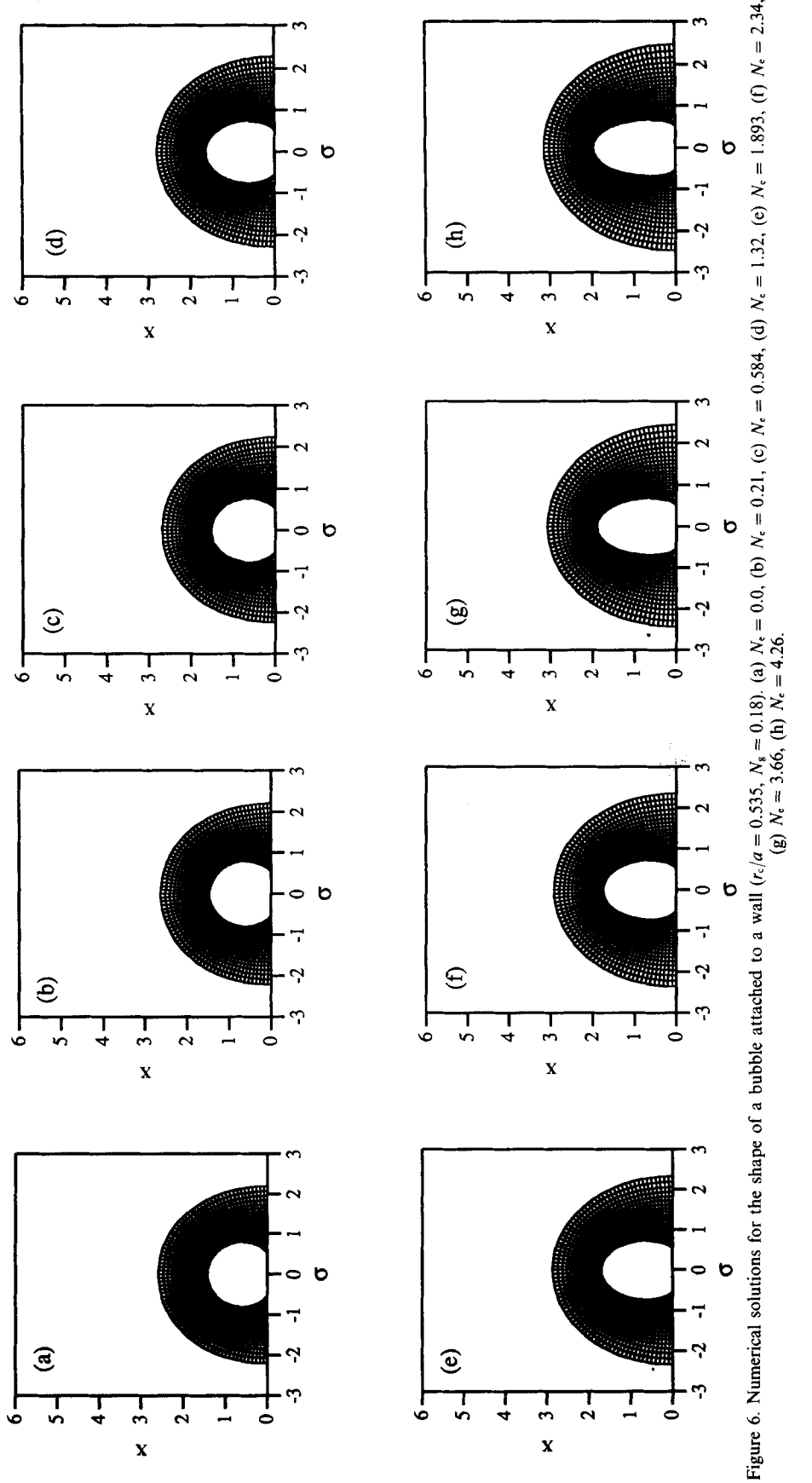

Figure 6. Numerical solutions for the shape of a bubble attached to a wall ($r_c/a = 0.535$, $N_g = 0.18$). (a) $N_e = 0.0$, (b) $N_e = 0.21$, (c) $N_e = 0.584$, (d) $N_e = 1.32$, (e) $N_e = 1.893$, (f) $N_e = 2.34$, (g) $N_e = 3.66$, (h) $N_e = 4.26$.

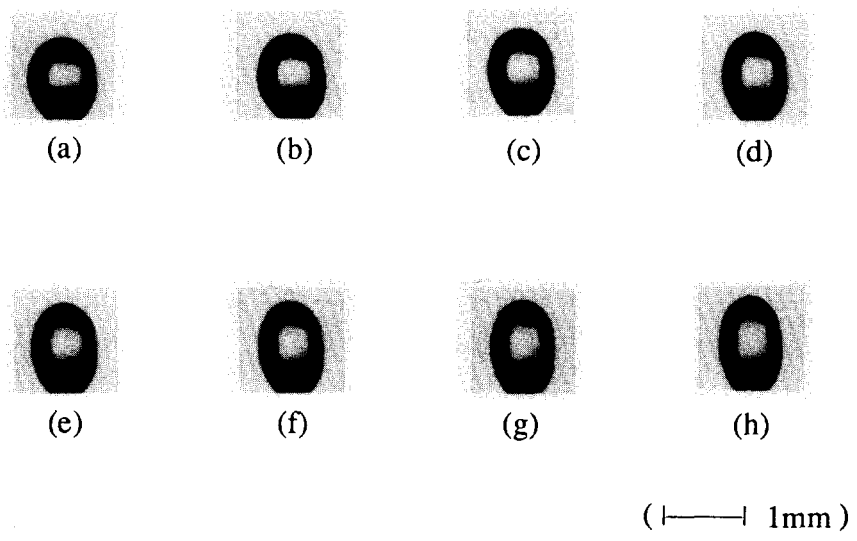

Figure 7. Experimental visualization of the shape of an air bubble attached to the lower electrode ($r_c/a = 0.535$, $N_g = 0.18$). (a) 0 kV ($N_e = 0.0$), (b) 6 kV ($N_e = 0.21$), (c) 10 kV ($N_e = 0.584$), (d) 15 kV ($N_e = 1.32$), (e) 18 kV ($N_e = 1.893$), (f) 20 kV ($N_e = 2.34$), (g) 25 kV ($N_e = 3.66$), (h) 27 kV ($N_e = 4.26$).

where F_b is the $\mathbf{e}_x$ directional component of the buoyancy force, and F_s and F_e are the $-\mathbf{e}_x$ directional components of the surface tension and electric forces. In dimensional form, [33] can be written as

$$\Delta\rho \boldsymbol{g} V = 2\pi\gamma r_c \sin\theta_c + \int_A (-\mathbf{e}_x)\cdot(\mathbf{n}\cdot\mathbf{T}^e)\mathrm{d}A, \qquad [34]$$

where V and A denote the bubble volume and the bubble surface area at departure time. If the condition of fixed contact angle is assumed as in Cheng & Chaddock (1986), the electric field decreases the surface tension force because the contact radius decreases as shown in figure 10.

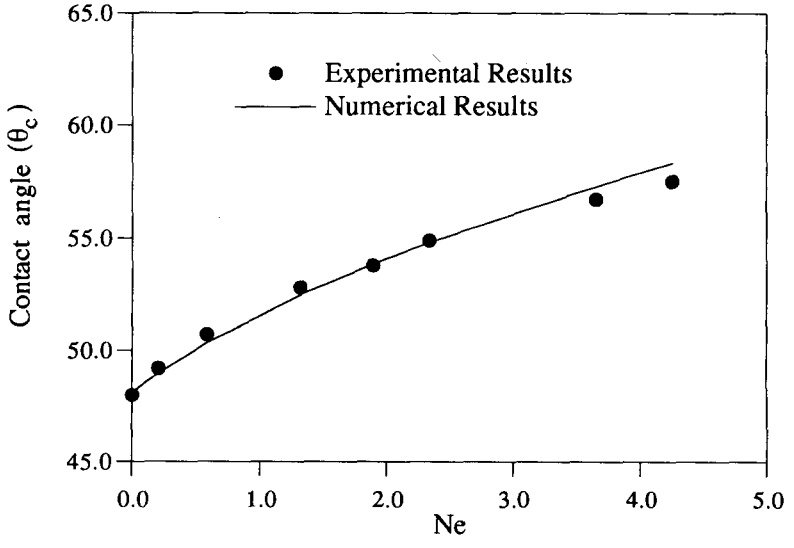

Figure 8. Comparison of the numerical and experimental results for variation of the contact angle with increase of N_e ($r_c/a = 0.535$, $N_g = 0.18$).

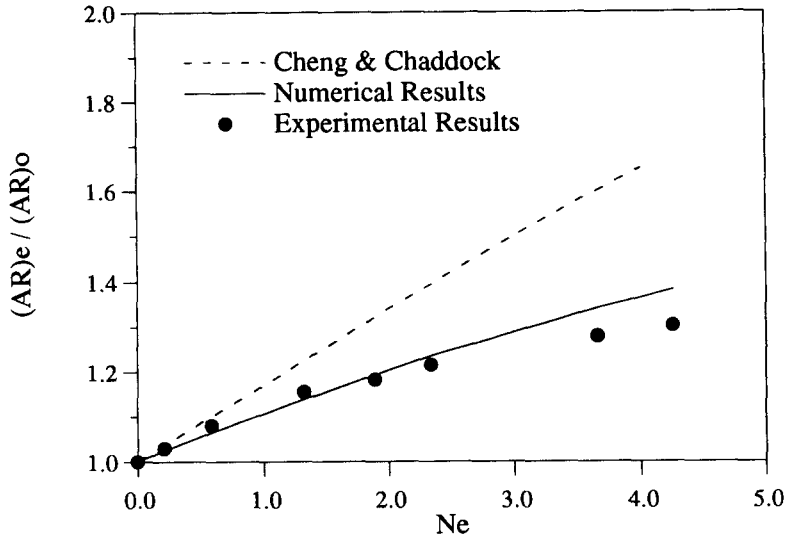

Figure 9. Comparison of the numerical and experimental results and the approximate prediction for variation of the aspect ratio with increase of N_e ($r_c/a = 0.535$, $N_g = 0.18$).

Therefore, if F_e exceeds the decrease in F_s ($F_e > |\Delta F_s|$), then the departure volume increases. If $F_e = |\Delta F_s|$, the departure volume remains unchanged. If $F_e < |\Delta F_s|$, the departure volume decreases.

In figure 11, the experimental results for the relative departure volume V/V_0, where V_0 is the departure volume in the absence of electric field, are shown. As shown in the figure, the relative departure volume is nearly constant over the entire range of the electric field strength that is considered. As mentioned above, the fact that the departure volume remains nearly constant means that the downward force exerted on the bubble surface due to the applied electric field is nearly the same as the decrease in the surface tension force due to contact radius decrease (i.e. $F_e \simeq |\Delta F_s|$). Numerical computations for determination of the departure volume have not been made. In order to compute the departure volume, the bubble growth problem must be considered. However, in this work, we have studied the effects of the electric field on the deformation of a bubble with a given volume. Currently, numerical studies on the bubble growth problem are being carried out in our group, and the results will be presented in the near future.

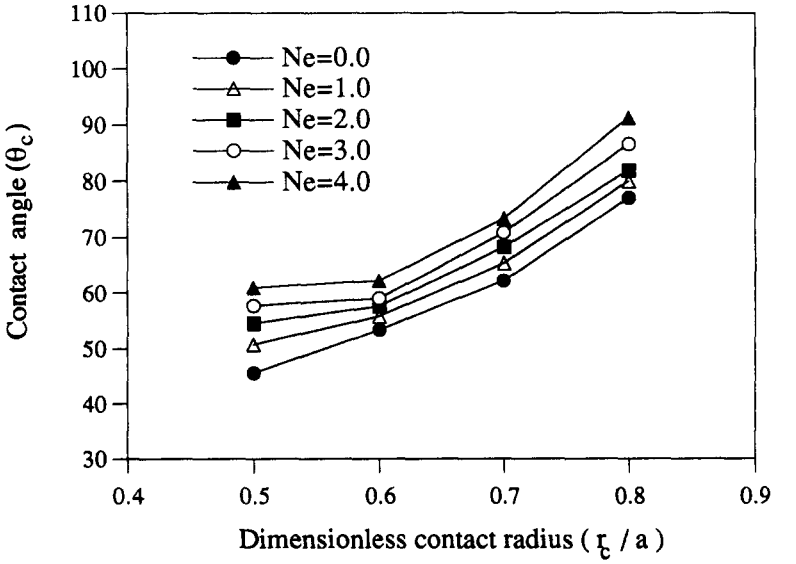

Figure 10. Plot of the contact angle vs the dimensionless contact radius for several N_e values ($N_g = 0.18$).

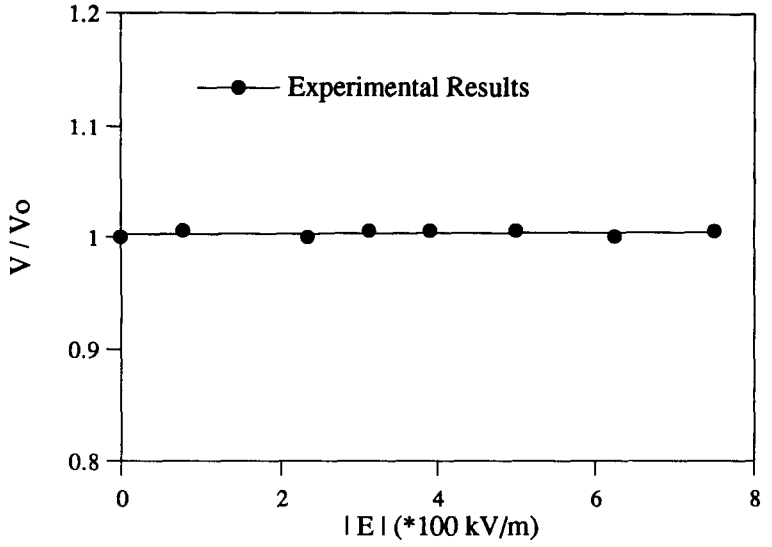

Figure 11. Experimental results for the relative bubble departure volume ($N_g = 0.183$–0.184).

6. CONCLUSIONS

To investigate the effects of a uniform electric field on an insulating bubble attached to a wall, numerical analyses and experiments are carried out. Fairly good agreements between the numerical and experimental results are obtained. When an electric field is applied, an air bubble on the lower electrode is found to be extended in the direction parallel to the imposed electric field. The elongation increases as the electric field strength increases. Consequently, the aspect ratio and the contact angle also increase with the increase of the electric field strength when the contact radius is fixed. On the other hand, the contact radius decreases as the electric field strength increases if the contact angle is fixed. It is observed experimentally that the bubble departure volume is nearly constant in a uniform electric field. This means that the downward electric force exerted on the bubble surface is nearly the same as the decrease in the surface tension force due to contact radius decrease under the imposed electric field.

Acknowledgements—This work was supported by grants from the Korea Institute of Machinery and Metals and the Advanced Fluids Engineering Research Center at the Pohang University of Science and Technology.

REFERENCES

Allen, P. H. G. & Cooper, P. 1987 The potential of electrically enhanced evaporators. *3rd Int. Symp. Large Scale Applications of Heat Pumps*, Oxford, 221–229.

Batchelor, G. K. 1967 *An Introduction to Fluid Dynamics*. Cambridge University Press, Cambridge.

Bonjour, E., Verdier, J. & Weil, L. 1962 Electroconvection effects on heat transfer. *Chem. Eng. Prog.* **58,** 63–66.

Chang, L. S. & Berg, J. C. 1985 The effect of interfacial tension gradients on the flow structure of single drops or bubbles translating in an electric field. *AIChE J.* **31,** 551–557.

Cheng, K. J. & Chaddock, J. B. 1984 Deformation and stability of drops and bubbles in an electric field. *Phys. Lett.* **106A,** 51–53.

Cheng, K. J. & Chaddock, J. B. 1986 Maximum size of bubbles during nucleate boiling in an electric field. *Int. J. Heat Fluid Flow* **7,** 278–282.

Choi, H. Y. 1962 Electrohydrodynamic boiling heat transfer. Ph.D. thesis, Department of Mechanical Engineering MIT.

Cooper, P. 1990 EHD enhancement of nucleate boiling. *Trans. ASME* **112,** 458–464.

Crowley, J. M. 1995 Dimensionless ratios in electrohydrodynamics. In *Handbook of Electrostatic Processes*, Ch. 7, 99–119. Marcel Dekker, New York.

Feng, J. Q. & Beard, K. V. 1991 Three-dimensional oscillation characteristics of electrostatically deformed drops. *J. Fluid Mech.* **227,** 429–447.

He, W. & Chang, J. S. 1995 EHD Enhanced mass transfer operations and chemical reactions. In *Handbook of Electrostatic Processes*, Ch. 24, 527–553. Marcel Dekker, New York.

Jones, T. B. 1978 Electrohydrodynamically enhanced heat transfer in liquids—a review. *Adv. Heat Transfer* **14,** 107–148.

Kang, I. S. & Leal, L. G. 1987 Numerical solution of axisymmetric, unsteady free boundary problems at finite Reynolds number I. Deformation of a bubble in a uniaxial straining flow. *Phys. Fluids* **30,** 1929–1940.

Lovenguth, R. F. & Hanesian, D. 1971 Boiling heat transfer in the presence of nonuniform direct current electric fields. *Ind. Eng. Chem. Fundam.* **10,** 570–576.

Markel, M. & Durfee, R. L. 1965 Studies of boiling heat transfer with electric fields. *AIChE J.* **11,** 716–723.

Melcher, J. R. & Taylor, G. I. 1969 Electrohydrodynamics: a review of the role of interfacial shear stresses. *Ann. Rev. Fluid Mechanics* **1,** 111–146.

Ogata, J. & Yabe, A. 1991 Augmentation of nucleate boiling heat transfer by applying electric fields: EHD behavior of boiling bubble. *ASME/JSME Thermal Eng. Proc.* **3,** 41–46.

Ogata, J. & Yabe, A. 1993 Basic study on the enhancement of nucleate boiling heat transfer by applying electric fields. *Int. J. Heat Mass Transfer* **36,** 775–782.

Ryskin, G. & Leal, L. G. 1983 Orthogonal mapping. *J. Comput. Phys.* **50,** 71–100.

Ryskin, G. & Leal, L. G. 1984 Numerical solution of free-boundary problems in fluid mechanics. Part 1. The finite-difference technique. *J. Fluid Mech.* **148,** 1–17.

Wohlhuter, F. K. & Basaran, O. A. 1992 Shapes and stability of pendant and sessile dielectric drops in an electric field. *J. Fluid Mech.* **235,** 481–510.

Zanin, A. I. 1987 Kinetics of boiling of a superheated liquid in an electric field. *Heat Transfer Soviet Res.* **19,** 16–21.